REPORT DOCUMENTATION PAGE

Form Approved
OMB No. 0704-0188

1. REPORT DATE *(DD-MM-YYYY)*	**2. REPORT TYPE**	**3. DATES COVERED** *(From - To)*
May 2013	Technical Paper	May 2013-June 2013

4. TITLE AND SUBTITLE
The use of x-ray radiography for measuring mass distributions of Rocket Injectors

5a. CONTRACT NUMBER
N/A

5b. GRANT NUMBER

5c. PROGRAM ELEMENT NUMBER

6. AUTHOR(S)
S.A. Schumaker, A.L. Kastengren, M.D.A. Lightfoot and S.A. Danczyk

5d. PROJECT NUMBER

5e. TASK NUMBER

5f. WORK UNIT NUMBER
Q0X3

7. PERFORMING ORGANIZATION NAME(S) AND ADDRESS(ES)

Air Force Research Laboratory (AFMC)
AFRL/RQRC
10 E. Saturn Blvd.
Edwards AFB CA 93524-7680

8. PERFORMING ORGANIZATION REPORT NO.

9. SPONSORING / MONITORING AGENCY NAME(S) AND ADDRESS(ES)
Air Force Research Laboratory (AFMC)
AFRL/RQR
5 Pollux Drive
Edwards AFB CA 93524-7048

10. SPONSOR/MONITOR'S ACRONYM(S)

11. SPONSOR/MONITOR'S REPORT NUMBER(S)
AFRL-RQ-ED-TP-2013-126

12. DISTRIBUTION / AVAILABILITY STATEMENT
Distribution A: Approved for Public Release; Distribution Unlimited. PA#13299

13. SUPPLEMENTARY NOTES
Conference paper for the JANNAF (7th LPS section), Colorado Springs, CO, June 2013.

14. ABSTRACT
Current limitations in available data and computational tools have led to an on-going reliance on experimental measurements for injector design. Unfortunately, the mass flow rates typically encountered in rocket engines create sprays with high optical densities and render the vast majority of optical and laser techniques ineffective. Data has been obtainable through mechanical patternation, but the technique has limitations especially near the injector. Time-gated ballistic imaging has also shown promise in rocket injectors but produces only qualitative information about the mass flux. An x-ray radiographic technique with a high-power x-ray source (the Advanced Photon Source at Argonne National Laboratory) has been applied to these highoptical- density sprays. To achieve this testing a mobile flow facility was constructed; this facility simulates the rocket flows using water and nitrogen instead of fuel and oxidizer. The x-ray radiography technique can be applied in two ways. Time-averaged measurements provide information related to the mass flux and droplet velocity while time-resolved measurements have the ability to provide droplet size and velocity distributions. Both techniques have been applied toa specific injector type of interest in rocket propulsion, a gas-centered swirl-coaxial injector, andthe results are used to show the complexities and strengths of x-ray radiography and illustrate the types of useful information that can be extracted, information that will aid in the development and improvement of rocket injectors.

15. SUBJECT TERMS

16. SECURITY CLASSIFICATION OF:			**17. LIMITATION OF ABSTRACT**	**18. NUMBER OF PAGES**	**19a. NAME OF RESPONSIBLE PERSON**
					Alex Schumaker
a. REPORT	**b. ABSTRACT**	**c. THIS PAGE**	SAR	18	**19b. TELEPHONE NO** *(include area code)*
Unclassified	**Unclassified**	**Unclassified**			661-525-5165

Standard Form 298 (Rev. 8-98)
Prescribed by ANSI Std. 239.18

THE USE OF X-RAY RADIOGRAPHY FOR MEASURING MASS DISTRIBUTIONS OF ROCKET INJECTORS

S.A. Schumaker[1], A.L. Kastengren[2], M.D.A. Lightfoot[1] and S.A. Danczyk[1]
[1]Air Force Research Laboratory, Edwards AFB, CA, USA
[2]Argonne National Laboratory, Argonne, IL, USA

ABSTRACT

Current limitations in available data and computational tools have led to an on-going reliance on experimental measurements for injector design. Unfortunately, the mass flow rates typically encountered in rocket engines create sprays with high optical densities and render the vast majority of optical and laser techniques ineffective. Data has been obtainable through mechanical patternation, but the technique has limitations especially near the injector. Time-gated ballistic imaging has also shown promise in rocket injectors but produces only qualitative information about the mass flux. An x-ray radiographic technique with a high-power x-ray source (the Advanced Photon Source at Argonne National Laboratory) has been applied to these high-optical-density sprays. To achieve this testing a mobile flow facility was constructed; this facility simulates the rocket flows using water and nitrogen instead of fuel and oxidizer. The x-ray radiography technique can be applied in two ways. Time-averaged measurements provide information related to the mass flux and droplet velocity while time-resolved measurements have the ability to provide droplet size and velocity distributions. Both techniques have been applied to a specific injector type of interest in rocket propulsion, a gas-centered swirl-coaxial injector, and the results are used to show the complexities and strengths of x-ray radiography and illustrate the types of useful information that can be extracted, information that will aid in the development and improvement of rocket injectors.

INTRODUCTION

The design process of “build, bust, rebuild” is no longer feasible. Engine subcomponents must be highly evolved prior to integration testing at the mid- or full-scale. Unfortunately, large risks still exist for many liquid rocket subcomponent designs. When new cycles or revolutionary improvements are sought, the risks are very large. Risk reduction is, therefore, a major component of any engine-design program.

Ideally, designs could be conceived and tested computationally and well understood prior to any experimental work. Current computational models, however, are not yet able to simulate a full engine with the required level of confidence and fidelity. Even at the subcomponent level, computational simulations cannot yet be used independently for many components. With the current level of maturity of computational models, the uncertainty in modeling novel subcomponents or new cycles does not allow much risk reduction. Before they can be used, the simulations must be anchored and/or validated for conditions and devices similar to those being designed. Experimental work, then, is necessary.

To remedy the contradiction between the necessity and unaffordability of experiments, simplifications of experiments must occur. A common simplification is to focus on a specific subcomponent in isolation, such as the injector. Studies of injectors are typically further simplified by considering only one single injector out of the hundreds or thousands in a full-scale engine [1]. An additional simplification removes the combustion aspect of the operation. For liquid-gas injectors, such as those utilized in many engines [2], measurements of the breakup of the liquid can provide a good indication of overall engine performance without the need for more costly combustion experiments [1,3].

The quantitative data necessary to reduce risk is not available for many types of rocket injectors. Gathering these data is difficult due to the large optical densities of these sprays. Injectors with strong gas-phase participation, such as those utilized in oxidizer-rich cycles, have particularly large optical densities. In general, the near-injector region of nearly all atomizers is optically dense and measurements there are extremely difficult or impossible. The near-injector region is very important in rocket engines, however, because this area is typically where the flame is located. Understanding the spray characteristics in the combustion region is critical for predicting the flame behavior and the performance of the engine. Currently, spray characteristics and likely combustion performance is often extrapolated from downstream measurements; the errors accrued due to these extrapolations are not understood and have not been quantified. A well-developed set of design criteria relating performance to injector geometry and operation will lead to a reduction in engine development costs.

Several methods for making spray measurements exist, but they have severe limitations in the near-injector region. The high-optical density of the sprays results in multiple scattering of photons and renders visible-light techniques ineffective. Phase-Doppler Particle Analysis (PDPA), shadowgraphy, laser absorption and laser diffraction techniques all suffer from these multiple-scattering problems [4, 5]. Ballistic imaging is a cutting-edge technique that essentially removes multiply scattered photons [6], but it has limited signal-to-noise ratio and, being essentially shadowgraphy, is limited to qualitative or, at best, semi-quantitative images. Using a flow splitter is possible to enable visible-light techniques, but this approach disrupts the spray and has an unknown impact on the measurements. Similarly, mechanical patternation is possible for optically-dense sprays but is intrusive and can greatly alter the flow field. Intrusive effects are particularly strong near the injector exit and in the high flow rate conditions found in rocket injectors. To further a physics-based understanding of rocket injectors a quantitative nonintrusive diagnostic technique that does not suffer from multiple-scattering effects is required.

The dominant interaction of x-ray photons with droplets is absorption rather than the elastic scattering that occurs with visible light. X-ray radiography is, therefore, a possible quantitative diagnostic that does not suffer from multiple-scattering effects. Beer's Law can be used to determine the liquid-phase thickness along an integrated path length. This technique has recently been successfully applied to diesel injectors, aerated liquid jets and impinging-jet sprays [7-10]. X-ray radiography can be performed using either a bright monochromatic source, such as a synchrotron source, or a polychromatic source, such as a tube source; however, a synchrotron source has a number of well-documented advantages over a tube source [11]. The one large disadvantage of a synchrotron source is that the experiment must be brought to a synchrotron facility. Such facilities typically lack the infrastructure necessary to deliver high-pressure liquid and gas at sufficient flow rates for rocket injector testing. To overcome this limitation, a mobile flow facility was used. The facility was transported to the synchrotron source at Argonne National Laboratory's Advanced Photon Source (APS).

The prior x-ray radiography work cited above has focused on the intact, evolving, liquid core [7-10]. The current work differs in its focus on the mass flux and distribution for a spray (i.e., field of droplets) with essentially steady flow. Additional complexities are introduced to the technique when a number of moving, discrete objects (such as with a fully atomized spray) are being measured instead of an intact liquid core. These complexities occur because the measurement of equivalent path length (EPL) is a function of both droplet velocity and droplet size. However, additional possibilities are also present, such as providing discrete information about the amount of liquid within the line-of-sight of the x-ray beam at a given instance in time: this information includes size, velocity and number of droplets.

X-ray radiography is examined from the example of the near-injector region of several gas-centered swirl coaxial (GCSC) injectors. These injectors have been of interest in oxidizer-rich staged combustion cycles. The example measurements are used to demonstrate the capabilities of x-ray radiography as applied to optically-dense sprays. Previous work on GCSC injectors, including the development of physics-based scaling laws from shadowgraphy and similar imaging techniques, is used as a comparative basis [12, 13]. The x-ray radiography measurements are the first quantitative measurements of GCSC injector sprays in the near

injector region. This paper emphasizes the capabilities and complexities of the diagnostic with regard to spray measurements and not the behavior of the injector. The useful injector information that is obtained includes indications of previously unknown asymmetries and demonstrations of a less dense and/or faster-moving spray core and changes in the spray related to alterations of the injector geometry. Overall, this diagnostic represents a leap forward in measurement capabilities in dense sprays.

EXPERIMENTAL METHODS

GAS-CENTERED SWIRL COAXIAL INJECTORS

The spray studied here is produced by a GCSC injector (Fig. 1). This injector utilizes an axial, fast-moving gas stream to strip droplets from a swirling, wall bounded film. Unswirled gas enters down the centerline of the injector while the film is created by introducing liquid through holes tangentially drilled into the injector cup. This type of injector was originally designed to operate with liquid hydrocarbon and gaseous oxygen. In the interest of safety and simplicity, the cold-flow experiments reported here have been performed using demineralized water and gaseous nitrogen.

The injector is modular consisting of a stainless steel gas plenum and post and an acrylic injector body. An acrylic insert forms the last portion of the gas post and the initial shelter for the liquid. Four geometries are considered here as given in Table 1. Table 2 provides the range of operating conditions. Previous imaging studies of the injectors' interior showed that the film thickness was immeasurably thin prior to the injector exit at all but the lowest momentum flux ratio examined [12]. As a result, only droplets and relatively discrete ligaments are expected at the x-ray measurement locations (all located outside of the injector cup). Momentum flux ratio is the main scaling parameter of these injectors as demonstrated in earlier work [13]. The momentum flux ratio is defined as

$$\Phi = \frac{\rho_g v_g^2}{\rho_l v_l^2} \tag{1}$$

where ρ is the density and *v* the velocity with *g* denoting gas values and *l* liquid values. The complex compressible flow within the injector creates difficulties in the definition of a velocity for use in the momentum flux ratio definition. Details on the exact definitions can be found in an earlier work [13].

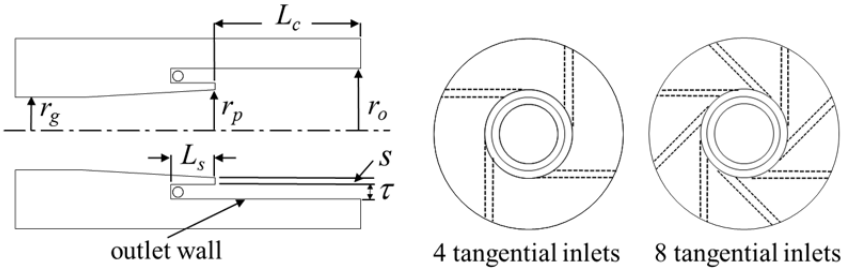

Figure 1. This sketch of a GCSC injector contains nomenclature for the important geometric dimensions found in Table 1.

Table 1. The different geometries are defined. The inlet area and number of inlets are varied to change the swirl level. The two are denoted by A_{in} and N_{in}, respectively.

Injector	r_o (mm)	r_p (mm)	L_c (mm)	L_s (mm)	τ (mm)	s (mm)	A_{in} (mm^2)	N_{in}
4H	9.53	6.35	33.0	3.17	1.65	1.52	7.54	4
8HDA	9.53	6.35	33.0	3.17	1.65	1.52	15.1	8
8HSA	9.53	6.35	33.0	3.17	1.65	1.52	7.50	8
OD	7.62	6.35	33.0	3.17	1.65	1.52	7.54	4

Table 2. Test Conditions.

Condition	m_g (g/s)	m_l (g/s)	Φ
4H-60	46	37	58
4H-90	46	30	86
4H-120	46	26	117
4H-145	46	23	141
8HDA-60	46	49	60
8HDA-90	46	40	91
8HDA-120	46	35	118
8HSA-60	46	32	58
8HSA-90	46	26	89
8HSA-120	46	22	120
OD-45	36	43	44

MOBILE FLOW LABORATORY (MFL)

No flow facility capable of producing the needed gas and liquid flow rates was available at a synchrotron x-ray source. Consequently, a facility was constructed by the Air Force Research Laboratory and transported to Argonne National Laboratory. This facility is designed to allow aerospace-propulsion injector testing at remote diagnostic facilities that do not have the infrastructure to provide relevant flow conditions. The MFL is a self-contained system with its own data acquisition and control systems allowing the entire experiment to be run remotely. Liquid nitrogen, electrical power and an exhaust system are all that is required of the host facility. Gaseous nitrogen is produced by using a cryogenic pump to increase the pressure of liquid nitrogen, supplied from either a drop or Dewar, to 408 atm. The high-pressure liquid nitrogen is then vaporized using a 24 kW electric vaporizer. Gaseous nitrogen is stored in two, 57-liter gas bottles. The flow system is designed to allow both bottles to be used in a blow down configuration or to run from one bottle while the other bottle is being filled. The gaseous nitrogen is also used to pressurize a 57 liter water tank. The available water was sufficient to complete several measurements prior to refilling the tank and it was possible to pause the data collection between measurement points to refill if needed.

The MFL is capable of delivering water and gaseous nitrogen on the order of 450 g/s at pressures in excess of 130 atm. Calibrated critical-flow orifices were used to meter the gas and liquid flow rates with an uncertainty of approximately 4% and 0.5%, respectively. These uncertainties are largely driven by the uncertainty in the temperature [14]. Gas and liquid flow rates are controlled using electronic pressure regulators.

The nature of the beamline setup at the Advanced Photon Source (APS) required operating the injector in a horizontal orientation and using a semi-enclosed collection and vent system. This configuration differs from tests previously conducted using these injectors (vertical orientation with open exhaust [12, 13]). The exhaust typically operated at 8.5 m^3/s. The limited space in the 7-BM beamline necessitated a curved exhaust duct. The distance from the spray to

the back, curved surface of the exhaust duct was on the order of one meter. Because of the exhaust capabilities and to limit splash back of water (caused, in part, to the curved geometry of the outlet), gas flow rates in these tests were limited to ~46 g/s, well below the maximum capabilities of the system.

X-RAY RADIOGRAPHY

Experiments were conducted at Argonne National Laboratory's Advanced Photon Source (APS) in beamline 7-BM. This location has been conducting x-ray radiographic studies of sprays for several years [7-10]. The x-rays are produced by a synchrotron bending magnet and, as such, the raw (white beam) radiation is polychromatic and nearly collimated. Prior to use in radiographic studies, the beam is conditioned using a monochromator to create a monochromatic beam ($\Delta E/E=1.4\%$). The beam is then focused to create a 5 by 6 μm FWHM (full width half maximum) beam at its narrowest point using a pair of Kirkpatrick-Baez focusing mirrors housed in the experimental enclosure. The beam has a flux of 1.6×10^{10} photons per second after the experimental apparatus and was tuned to 10 keV of photon energy.

Measurements are made using a titanium foil and a silicon PIN diode as detectors. The titanium foil detector uses the x-ray fluorescence from a thin (0.5 μm) sheet of titanium placed in the x-ray beam to monitor the incident x-ray intensity on the experiment. The PIN diode measures the intensity after the beam has traveled through the spray. For the time-averaged data the photo-current from this PIN diode is amplified and time averaged over a 4 second integration window at each measurement location. The time-resolved data was collected from the diode at 1 MHz, and the signal was conditioned with a second-order low pass filter with a -3dB frequency of 300 kHz. Eight seconds of data are collected at each measurement location.

The recorded signal level is converted to an Equivalent Path Length (EPL) of water using Beer's law

$$EPL = \frac{-\ln(I/I_0)}{\beta\rho} \tag{2}$$

where I is the intensity of the transmitted light (from the PIN diode), I_0 is the intensity of incident light, β is the mass attenuation coefficient, and ρ is the density of the absorbing fluid. EPL can also be converted to a projected liquid mass density by multiplying by the liquid density. Normalization by I_0 was performed in two steps. First, each point in the scan was normalized by a corresponding beam intensity measured from the titanium foil. The I_0 measurement accounts for changes in beam intensity during a scan, a natural result of the manner in which the synchrotron operates. A time-averaged scan across the spray width at one axial location took approximately 8 minutes. The second normalization baselines the intensity to the zero-absorption case. For the time-averaged data the average of 0.5% of the scan points with the highest transmissions were used to calculate this baseline; in the time-resolved data 1% of the points were used. The mass attenuation coefficient, β, can be calculated using the NIST photon cross section database [15]: for pure water and a beam energy of 10 keV, β is 5.33 cm^2/g. The EPL is the path length-integral of the amount of water in the beam. Interpretation of the EPL is discussed in detail in the Results and Discussion section. It should be noted that the use of monochromatic x-rays greatly simplifies the conversion of x-ray transmission to EPL [11]; this is a significant advantage of synchrotron sources over laboratory x-ray sources.

A programmable linear translation stage was used to accurately position the spray relative to the fixed beam. Scans were made across the width of the spray, perpendicular to the injector axis, at several downstream locations. The distance between measurement points, width of the measurement area and other details varied depending on whether the measurements were time-averaged or time-resolved.

RESULTS AND DISCUSSION

Two types of measurements were made in this study—time-averaged and time-resolved. Some details of the time-averaged and time-resolved experiments differ. Important specifics are summarized in Table 3. The main difference is that each measurement was integrated over 4 seconds for the time-averaged data while the integration time for the time-resolved data was 1 microsecond. Substantially more time-averaged measurements were taken than time-resolved measurements. Data transfer times for the time-resolved data was the limiting factor; this limitation has since been improved with the implementation of a different data acquisition system. Wetting of the injector outlet and occasional pendant droplets limited how near to the injector measurements could be taken: the closest measurements were limited to 3 mm downstream of the injector outlet. This location is still well inside the near-injector region: for comparison, PDPA measurements (a conventional laser diagnostic) of these GCSC injectors are difficult at 20 mm downstream and impossible at closer distances.

For both types of measurements, the incident radiation is converted to an equivalent path length (EPL) as described above. This EPL can be roughly conceptualized as the thickness of water that is in the beam, on average, over a given time period. Again, for the time-averaged data this time period is several seconds while the time period is a microsecond for the time-resolved measurements. In terms of flow variables, time averaged EPL is a function of the local mass flux and velocity and for an area of uniform mass flux and velocity

$$EPL = \frac{JL}{V\rho}, \tag{3}$$

where *J* is the mass flux, V is the velocity of the liquid phase, and L is the pathlength of the area. If the only data available is time-averaged EPL, then changes in velocity cannot be distinguished from changes in mass flux. Additional information to differentiate the two could come from other techniques, such as mechanical patternation, but as cited above these tend to be impractical or impossible in the near-injector region. However the additional information to differentiate between velocity and mass flux could be extracted from time-resolved x-ray radiography measurements.

In the case of time resolved measurements, the instantaneous EPL is also a function of droplet size. One way to demonstrate the interdependence between droplet size and velocity for time resolved measurements is to consider a single droplet moving through the beam. Figure 2 shows representative time-resolved EPL for single droplets. In the time-resolved signal of a single droplet, the peak height of the EPL corresponds to the droplet diameter while the width of the signal and the amount of time the signal departs from zero are related to both the droplet velocity and the droplet diameter. The blue solid line in Fig. 2 is the signal for a 50 μm droplet moving at 1 m/s while the black dotted line is the same size droplet moving at 4 m/s. While the peak of both signals is the same, the width of the signal differs. Both the time-resolved and time-averaged results will change as the velocity of the liquid phase changes. Similarly, two droplets can have differing time-resolved signals but identical time-averaged EPL when averaged over only a few droplet events. The red dashed line in Fig. 2 has the same time-averaged EPL as the 50 μm droplet traveling at 1 m/s, ~38 μm, but it is created from a 100 μm droplet with a velocity of 4 m/s. The single droplet is an extreme case, yet the results are illustrative of the challenges found when interpreting the EPL of sprays.

Table 3. Measurement specifics for the two types of x-ray radiography measurements

Type	Width (mm)	Step Size (mm)	Axial Locations (mm)	Angles (°)	Integration Time (s)
Averaged	48.5	0.5	3, 5, 7.5, 10 and 20	0, 60, and 300 or every 30	4
Resolved	33.0	1.0	3 and 5	0	$1x10^{-6}$

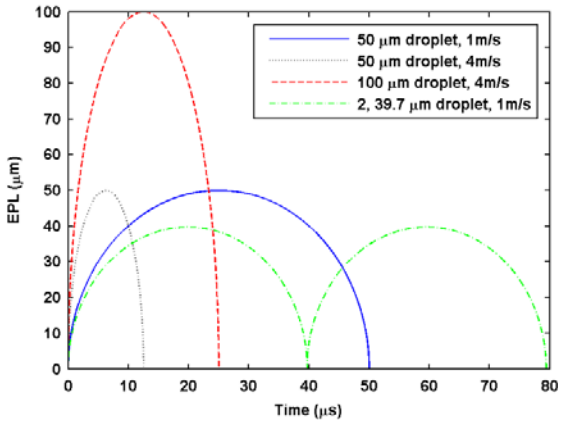

Figure 2. The time-resolved EPL of a single droplet changes with the droplet size and velocity.

While looking at a single droplet falling through the beam is in general a simplification of the spray case, it adds a volumetric effect that does not occur in the spray, since in the above examples the beam was assumed to transverse the center of the droplet. As the droplet diameter changes, the volume changes with the radius to the 3rd power, while the pathlength of the beam changes by 2 times the radius. For example, if a single droplet is split into two droplets with the mass flux and velocity held constant, the average EPL will differ. Such a case is illustrated in Fig. 2 by the blue and green lines. The same mass flux is divided between a single, 50 μm droplet traveling at 1 m/s or two 39.7 μm droplets also traveling at 1 m/s but entering one immediately after the other. The time-averaged EPL in the first case is just over 24.7 μm while it is just under 62.4 μm in the second instance. The volumetric effect does not occur in the time averaged measurements of actual sprays because neighboring points (or the interpolation between neighboring points) account for the mass not measured at a single measurement location. For the time-resolved measurements this effect will introduce a bias that must be accounted for to make the method fully quantitative.

For rocket injectors, knowledge of the mass flux is important in determining atomization quality and uniformity. Items of interest that can be determined from mass flux include whether or not the spray is hollow and/or the amount of mass at the edges versus the center of the spray cone. The interdependence of velocity and mass flux in the EPL measurements does, however, make these assessments challenging. A further set of examples is provided here to further explain the effects of this complication on spray interpretation. Figure 3a shows EPL profiles created artificially and compared to test condition 8HSA-120. A simple Matlab [16] program was written to simulate the x-ray radiography measurement process and results. This program simulates a spray with a predefined axially symmetric mass flux and velocity distribution. These distributions are then mapped to a structured grid creating an artificial axisymmetric spray. The size of each grid cell and the local value of mass flux and velocity are then used in Eqn. 3 to calculate the local EPL. The EPL is then summed across the spray to simulate the pathlength integration of the measurement technique. For all of the cases illustrated in Fig. 3a the mass flux and the mass averaged velocity is the same as that for test condition 8HSA-120.

If the velocity and mass flux are uniform across the spray—that is, the spray is a uniform, solid cone—then the EPL is essentially a half ellipse, as shown in Fig. 3a by the Case 1 line. For reference, the mass flux and velocities used are given in Figs. 3b and 3c, respectively. If the spray is somewhat hollow then the mass flux is decremented in the center (see Case 3 in Fig. 3b). When the velocity is uniform this change in mass flux produces an EPL with a small dip at the center (Case 3, Fig. 3a). As a final example case, consider a solid cone spray—a uniform mass flux—where the droplets are traveling more rapidly at the center of the spray (Case 2 in Fig.3). The EPL of this example also shows a dip at the centerline. This depression is more pronounced and wider than the one created by the assumption of a nearly hollow cone with a uniform velocity profile.

Compare these three example cases to the data produced by a GCSC injector. The atomization, which occurs along the injector walls, is driven by a high-velocity gas core, so a boundary-layer-like velocity deficit is created at the edge of the spray, and an overall velocity distribution generically similar to that shown in Fig. 3c, Case 2 occurs. Patternation of similar injectors suggests that the mass distribution is nearly Gaussian [17] as is the example of the Case 3 in Fig. 3b. The axial location of droplet formation also impacts the droplet field. Droplets

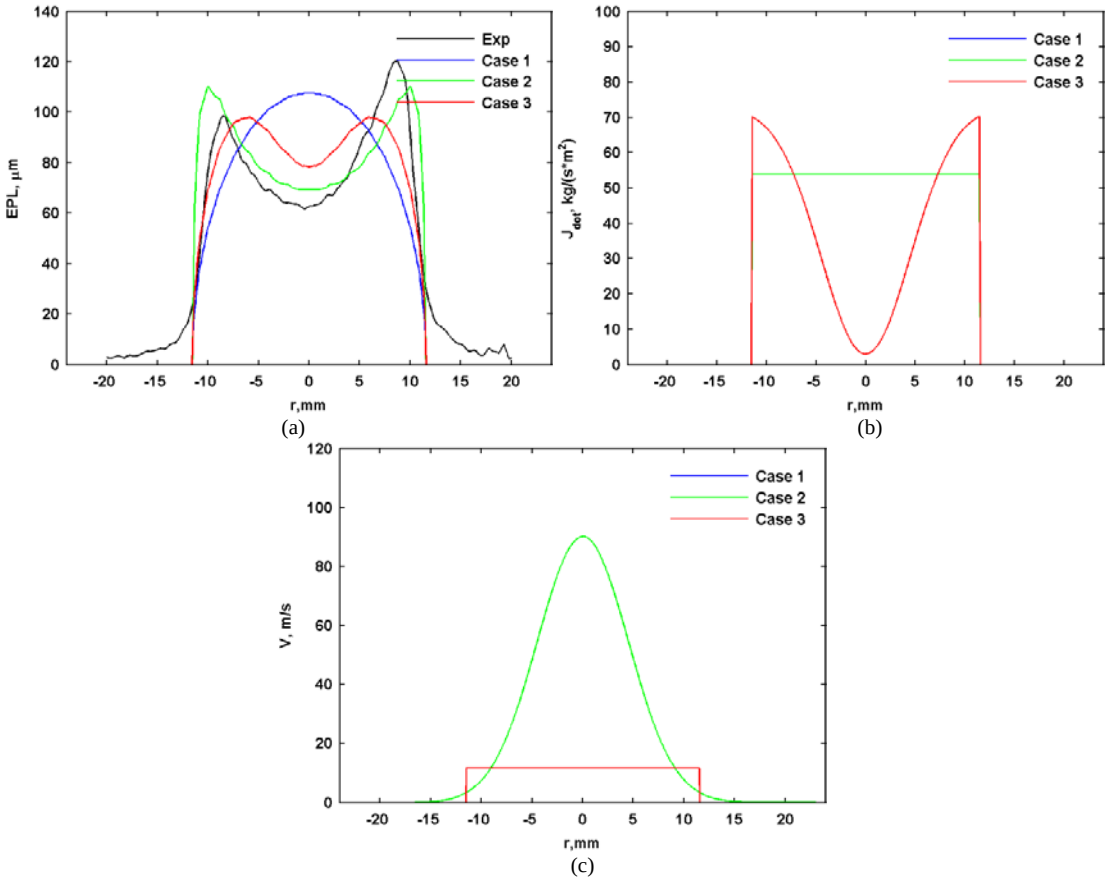

Figure 3. Artificially created EPL profiles compared to test condition 8HSA-120 5mm downstream (a) using various mass flux distributions (b) and velocity distributions (c). The results indicate that the valley in the center of the experimental EPL profile is largely driven by the higher velocity in the center of the spray. Note that in (b) Case 1 and 2 are identical and in (c) Case 1 and 3 are identical.

that have migrated to the center of the spray were likely formed early in the atomization process and therefore have had more time to accelerate and undergo secondary breakup (become smaller). The EPL of the experimental spray (8HSA-120) shows a large central depression. Is this depression caused by a distribution of mass flux or velocity or both? From the example cases, the velocity distribution has a bigger effect on the EPL and causes a depression with a similar size and width to the experimental case. The deficit in mass at the centerline causes a more shallow depression; even if the spray is considered to be truly hollow (zero mass at the centerline); the EPL is not sufficiently low to match the experimental data at the centerline. These findings strongly suggest that the spray does, indeed, have a higher velocity at its centerline. However, there is insufficient information to know if the spray also has a mass deficit in the spray center. While a mass deficit alone is unable to account for the change in EPL at the centerline, the EPL could be reproduced either with a velocity profile similar to the one for Case 2 in Fig. 3 alone or with a combination of a centerline mass deficit and a Gaussian velocity distribution. One final important limitation in the measurements is highlighted in these examples, especially Case 3: x-ray radiography is a line-of-sight measurement. As such, the peripheries of an axisymmetric spray contribute to the EPL across the entire spray width. The EPL will never go to zero, then, at the center of a conic spray even if the mass flux in the center is zero.

TIME-AVERAGED RESULTS

The experimental profile shown in Fig. 3a has the same general shape as the EPL profiles of all test conditions. They all have peaks on the edges of the spray and a trough in the middle. This bimodal shape indicates a higher average density at the spray periphery than at the spray center, but, again, this variation is likely caused by a combination of mass and velocity distributions, not by a centerline mass decrement alone. While this complication makes quantitative assessments difficult without additional information, the time-averaged results still provide information important to evaluating and understanding injector operations.

The time-averaged x-ray radiography results also offer confirmation and some quantification of trends and scaling found during earlier shadowgraphy experiments [12, 13, 18]. By taking several measurements at different axial distances, the evolution of the spray can be assessed. The EPL profiles, shown in Fig. 4 for condition 8HSA-90, allow a quantitative assessment of spray angle and the spreading of the spray with downstream distance. Similar information can be extracted from the shadowgraphy, but shadowgraphs and x-ray radiography are measuring different quantities. Additionally, the demarcation of the spray edge in the shadowgraphy is somewhat subjective and can be impacted by lighting levels while the x-ray radiography results are more quantitative and repeatable in nature. In general, both sets of results show that the cone angle is relatively small and is not constant over the downstream distance examined.

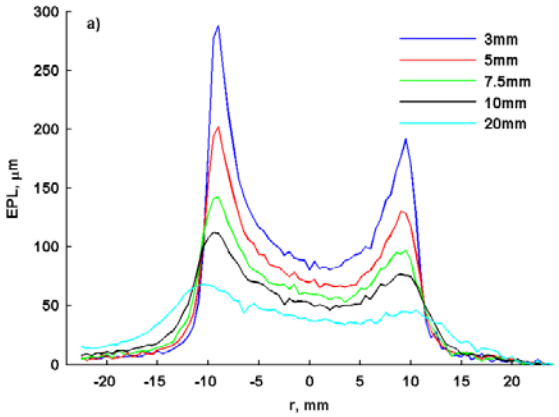

Figure 4. The EPL decreases as the measurement location moves downstream, but the width does not change appreciably in the near-injector region. (8HSA-90 is shown here at an radial orientation of 60°.)

The negligible increase in spray width accompanied by an overall EPL decrease in the near-injector region (Fig. 4) means that the droplets are undergoing acceleration here. For condition 8HSA-90 the spray width between 3 and 5 mm downstream is unchanged yet a decrease of 25 μm or more is seen throughout the entire EPL profile. Clearly, the overall mass flux is unchanged, so the EPL must be caused by an increase in the velocity. This change is EPL with a consistent width is observed throughout all tests in the near-injector region. The acceleration of the spray's mass can be quantified by considering the mass-weighted velocity at the various downstream locations. The mass-weighted velocity (V_{ma}) is obtained by dividing the liquid mass flow rate by the integral of the integrated average liquid density profile (i.e., the EPL profile) [19]. This double integral first integrates along the beam pathlength and then across the spray so that all liquid mass in the two-dimensional cross-section perpendicular to the injector axis is counted. Figure 5 shows V_{ma} for three injector geometries operating at a momentum flux ratio of approximately 120. As would be expected, operating conditions and geometries affect the V_{ma} and acceleration. For example, some geometries and conditions—such as a reduction in swirl—produce large slow-moving droplets on the spray periphery; these structures (observed in shadowgraphy of earlier experiments and shown in Fig. 6) would, on average, lower the mass-weighed velocity. Indeed, the condition with the lowest swirl, 8HDA, has the lowest mass-weighted average velocity. Mass-weighted velocities 3 mm downstream are between 6 and 8 m/s; the mass accelerates to between 17 and 20 m/s by 20 mm downstream. Even though the velocities near the injector are low relative to the exit gas post velocity these values indicate that substantial mass has, on average, undergone large accelerations. The liquid's axial velocity when it exits the sheltered area is ~0.5 m/s, so the droplets experience acceleration on the order of 1,000 m/s^2 by 3 mm from the exit. Between 3 and 10 mm downstream, acceleration is on the order of 10,000 m/s^2.

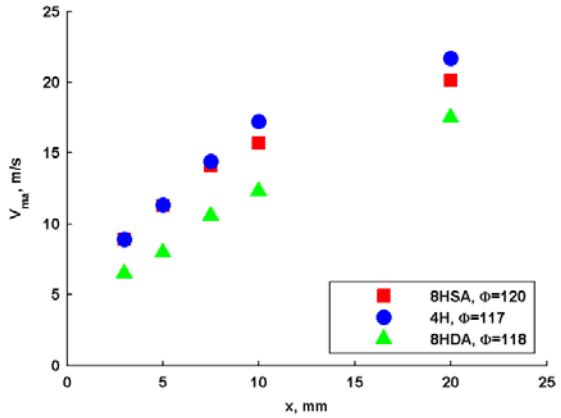

Figure 5. The spray accelerates as it moves downstream, as seen by the increase in mass-weighted velocity.

By 20 mm, acceleration appears to be decreasing, but a lack of data downstream makes it impossible to know where V_{ma} will asymptote. Note that conventional spray measurements in these GCSC injectors are limited to 20 mm or farther downstream. These limitations are common in many injectors, particularly for rocket operation. The x-ray results quantify the evolution of the spray in the near-field region—evolution which cannot be captured by conventional diagnostics but is approximated from extrapolations of downstream measurements. These extrapolations are common but produce unknown errors.

The time-averaged x-ray radiography results also confirm basic momentum flux ratio scaling trends reported earlier [13]. Images have indicated an increase in spray quality and atomization as the momentum flux ratio increases with a threshold value above which little change in quality is observed. Figure 7 shows the change in EPL from a single, representative injector geometry (4H at a radial orientation of 60^{o}) as the momentum flux ratio is altered. These spray improvements with increasing momentum flux ratio are clearly indicated in the EPL results as improvements in spray uniformity. Here the threshold value above with increases in momentum flux ratio produce minimal spray improvement is 120. The liquid flow rate was changed to achieve different momentum flux ratios resulting in different EPL magnitudes as the overall mass flux is altered. Because earlier scaling theories have shown that atomization efficiency is independent of liquid flow rate [18] the differences shown in Fig. 7 are related to the momentum flux ratio and not the liquid flow rate changes. The EPL results also provide quantitative comparisons for other changes in the injector such as inlet liquid swirl as shown with the V_{ma} results above and in examples contained within the Time-Resolved Results section below.

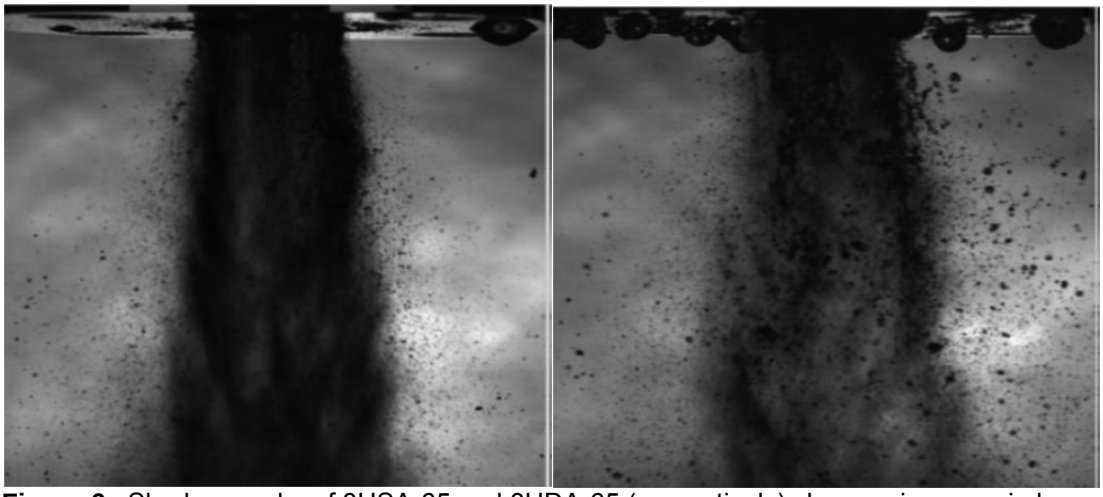

Figure 6. Shadowgraphs of 8HSA-65 and 8HDA-65 (respectively) show an increase in large, slow moving droplets at the spray periphery as the swirl number decreases

In addition to confirming shadowgraphy trends, the x-ray radiography provides an improved level of detail allowing added assessments. An overall appraisal of the data set indicates that most conditions have some level of asymmetry and that a single scan angle is insufficient to fully characterize the spray. Asymmetries were previously observed (via shadowgraphy) only at the lowest momentum flux ratio tested. Here, however, asymmetries are clearly visible over the full range of momentum flux ratios. While the nonuniformities are visible from the EPL profiles themselves (see Figs. 4 and 7), they are particularly visible from two-dimensional representations of the EPL in the near-injector region. Linear interpolation in the axial direction can be used to produce an image of EPL on a regular 500 μm grid (Fig. 8a). Multiple angular measurements can be combined at a single axial location to produce an image through linear interpolations onto an angular grid of 10° increments (Fig. 8b). These two-dimensional images make the asymmetries easier to see with the naked eye and highlight the complex three-dimensionality of the flow field. The axial slices through the spray, Fig. 8b, also show the slightly ovoid cross-section of the spray. These results clearly indicate the limitations of previous methods, such as shadowgraphy, that have not captured the nonuniformity, as well as the need for multiple angles to fully characterize the spray.

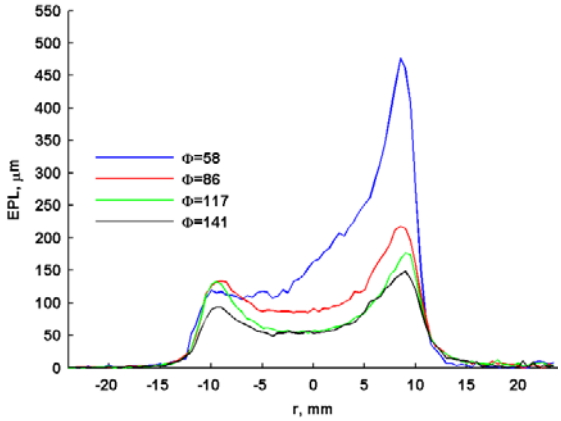

Figure 7. The spray uniformity increases as the momentum flux ratio increases. Injector geometry (4H) at a radial orientation of 60°.

While the time-averaged EPL does not provide a full story of the spray, it does provide substantial information not available with conventional diagnostics. These time-averaged results represent the first quantitative information available in GCSC sprays or any other type of shear driven spray. Time-averaged x-ray radiography can provide complementary information to conventional diagnostics as well as providing finer details on optically-dense sprays and their relationship to injector geometry and operating condition.

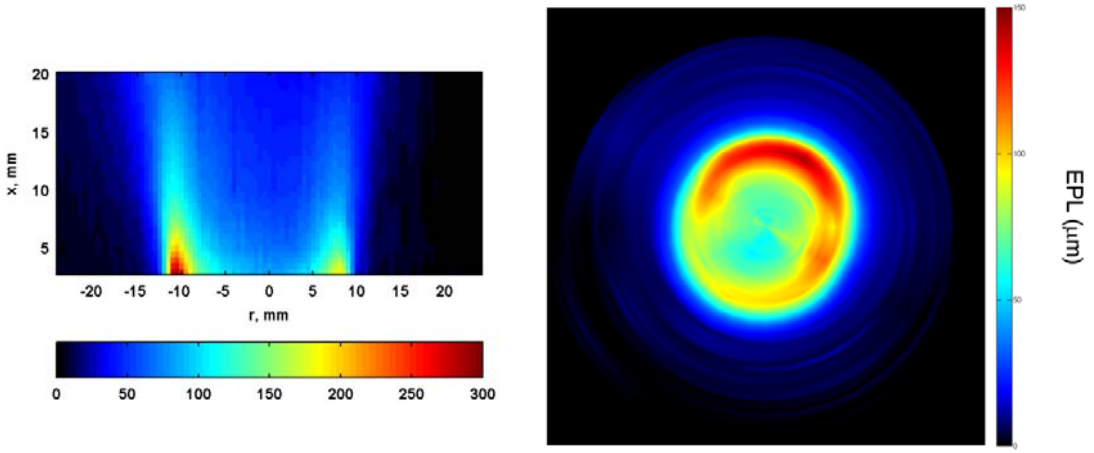

Figure 8. Nonuniformities are particularly visible when the EPL profiles are linearly interpolated to create two-dimensional images. Condition 8HSA-90 is shown as it varies in the axial direction (a) and as a function of angle (b). The slice across the spray axis is located 5 mm from the injector face.

TIME-RESOLVED RESULTS

As shown in Fig. 2, the time-resolved EPL corresponds to the droplet size and velocity. If a single droplet was in the x-ray beam at each instant then calculating the droplet size and velocity from the EPL would be trivial. The optical density and the line-of-sight nature of the measurement result in multiple droplets being within the beam at most instants in time. Sprays where a single droplet was in the beam at every instance would likely have optical densities that allowed conventional diagnostics to be applied. Despite multiple droplets existing within the probe volume, the peaks and departure time from zero (or between troughs in the signal) remain directly related to droplet diameter and velocity. Here a simple approach that ignores the effect that multiple droplets have on the EPL will be employed to develop spray statistics. While this simplification introduces errors and biases, it is sufficient to illustrate the potential of the x-ray radiography measurements for developing quantitative spray measurements.

Details on the simplified procedure and many of the biases introduced are presented in an earlier work [20] and summarized here for brevity. A Matlab program [16] was written to locate peaks and valleys within the time-resolved signal. Typically multiple peaks occur between times when the signal is at zero (Fig. 9) due to the multitude of droplets within the probe volume. As a simplification, when multiple peaks exist then the elapsed time is the measured time between troughs, even if the EPL does not start or return to zero. Elapsed times are likely underestimated in many cases as a result of this simplification leading to an increase in calculated velocity. The droplet diameter is determined by subtracting the value at each trough bounding the peak from the peak value; the maximum difference is kept. This simplification typically underestimates the droplet diameter when large numbers of droplets are present in the beam and overestimates it when only a few droplets are present. A few additional assumptions have been made for this simple analysis. There is a tacit assumption that particles traveling through the beam are spherical and, as such, have a single characteristic dimension. The process measures the maximum liquid thickness perpendicular to the injector axis, and an assumption has been made that the droplets are traveling perpendicular to the beam. For the GCSC injectors examined here, the gas velocity is dominant and predominately in the axial direction, so this assumption is likely to hold to a high degree except, possibly, on the extreme edges of the spray. Obviously, the current measurement only calculates the axial velocity component. The center of the droplet is assumed to travel through the beam so that the diameter is measured; off-center travel would result in a chord being measured instead, and the droplet would appear smaller than its true size. The temporal resolution and filtering of the signal create an upper threshold in the velocity that can be captured. Droplets with a velocity above this limit are not individually resolved with the current data-processing technique. The limit is a direct function of droplet size, and the maximum resolvable velocity for small droplets is lower than that for larger droplets. It should be noted that the current temporal resolution is well below the maximum available at the 7-BM beamline. The resolution was selected based on the ability to capture unsteadiness which was expected in some sprays rather than on the ability to resolve droplets traveling at high velocities. Based on the gas velocity and the calculated mass-weighted velocities, it is likely that a large number of droplets are not resolved as peaks in the current time-resolved measurements. Finally, the noise in the signal also creates a lower threshold in the discernible droplet diameter. Again, more about the impact of these assumptions can be found in a previous paper [20].

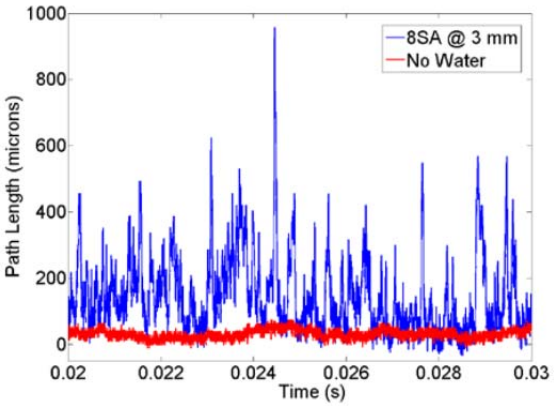

Figure 9. Large numbers of droplets, indicated by peaks in the time-resolved EPL, are seen in this 10 ms window of the filtered data.

Droplet diameters and velocities, i.e. spray statistics, are determined by applying the above method over 1 second of operation (1 million measurement points). Given the limitations in the current technique, particularly the velocity-size limitations, the distributions are likely to be strongly biased toward large and slow-moving droplets. The velocity threshold and other biases currently produce some results known to be untrue. For example, the droplets along the spray centerline have measured velocities below those on the periphery because the droplets in the core are often smaller and substantially faster than those at the edges, and, therefore, many centerline droplets are not being measured in the current set-up. Many of these limitations can be overcome. Yet even with the biases in place, the simplified process highlights the types of important injector information that can be extracted from time-resolved x-ray radiography.

An easy statistic to develop from the distributions is the mean droplet diameter. While related to the time-averaged EPL, the two are not identical. Figure 2 helps to illustrate these points—the mean of the curve is not the same as the droplet radius (half of the curve's maximum). Additionally, times of zero EPL are included in any average. Still, the qualitative behavior of the mean droplet diameter and the time-averaged EPL should be similar and offer some gauge of the trustworthiness of the measurements. The two results are given in Fig. 10 for condition 8HSA-90 at two downstream locations. The qualitative behavior and asymmetries are comparable for the time-averaged and mean droplet diameters despite the various limitations of the diameter measurement technique as currently applied. For a single droplet, excluding any time with no droplets in the beam, the time-averaged EPL is $\pi/4$ times the droplet diameter. However, as shown in Fig. 10, the calculated mean droplet diameter is larger than the time-averaged EPL. This discrepancy is expected since the current, simplified process does not resolve all droplets, particularly those that are small (and fast moving).

Not only do the mean droplet diameters vary at different locations within the spray, but the distribution of diameters also varies. The distribution of droplet diameters is an important parameter in the combustion of a spray, so of interest in propulsion injectors. A wide distribution is typically considered unfavorable because it extends the combustion zone as larger droplets take longer to evaporate, mix and combust than smaller droplets. Additionally, bimodal distributions are typically considered unfavorable. The droplet distribution at the right lobe (peak) within the time-average EPL, i.e. at +7mm from the centerline, and the distribution at the centerline differ, as shown in Fig. 11. The larger mean diameter at the periphery is caused by the wider distribution in droplet diameters. While a larger mean diameter could be predicted from the time-averaged EPL and was expected from earlier shadowgraphy (Fig. 6), the additional range of droplet diameters at the edge of the spray was not known. Data such as those shown in Fig. 11 will be able to provide quantitative droplet size information with improvements of the data capturing and processing systems. Again, signal-to-noise limitations and limitations in resolvable droplet velocities currently produces results biased towards larger droplet diameters.

The effects of some injector changes are also discernible from the droplet distributions. For example, shadowgraphy shows a wider array of droplet sizes with larger droplets at the periphery when the swirl level of the incoming liquid is decreased (Fig. 6) [18]. The droplet distributions from the time-resolved x-ray radiography also reflect this trend (Fig. 12): the mode and the width of the distribution increases as the swirl level decreases. Injectors with similar swirl levels, whose shadowgraphs are similar, have little difference in droplet distribution (Fig. 12). The velocity as a function of droplet diameter also changes; however, no independent comparator exists to assess the validity of the measured velocity trends. The time-resolved results also provide details on instabilities within the spray. Most of the sprays examined were steady, but one geometry and condition (OD-45) exhibited a noticeable unsteadiness. The time-resolved x-ray radiography results show periods of many, large droplets followed by periods of small, fewer droplets (Fig. 13). The frequency in the EPL corresponds to frequencies in the spray's boundary location determined from shadowgraphy studies [21]. The time-resolved data at the spray centerline suggests that there is a type of pulsing present that could cause chug instability in a rocket engine.

While the current data-processing technique of the time-resolved x-ray radiography remains oversimplified, the diagnostic is able to quantify changes in the spray caused by changes in injector geometry as well as provide additional details about the structure of spray instabilities. Eventually, the technique can be improved to provide Sauter mean diameters and diameter distributions. Improvements to the technique include improved curve fitting algorithms, increased data acquisition rate, decreased signal noise, and moving to a multiple pin diode detector (comparing multiple signals would aid in separating multiple droplets and characterizing which part of the droplet passed through the beam). These measures have long been used by injector designers in other fields [22] but are rarely available to rocket injector designers, particularly in locations where the combustion occurs.

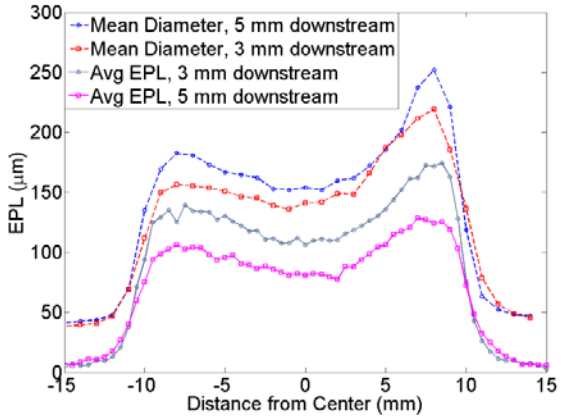

Figure 10. The behavior of the mean droplet diameter across the width of the spray is very similar to the time-averaged EPL.

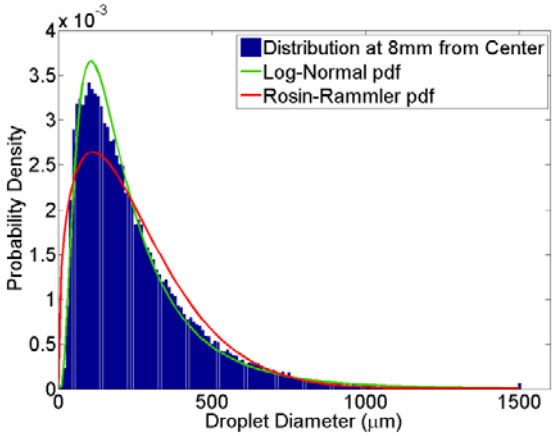

Figure 11. The droplet diameter distributions differ at the centerline and at 7 mm from the centerline (at the peak EPL value).

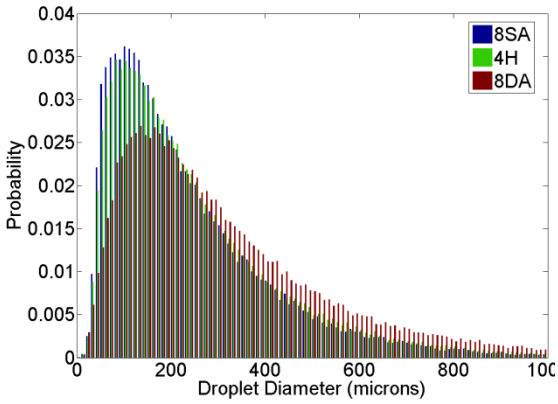

Figure 12. Droplet distributions clearly show a change to larger mean diameters and a wider range of sizes as the swirl number decreases (a). On the other hand, a change in liquid inlet has little or no impact on the diameter distributions (b). All geometries at $\Phi \approx 90$.

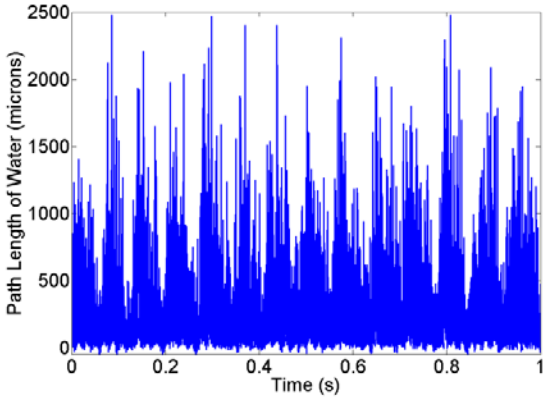

Figure 13. Spray unsteadiness is evinced through periods of large droplets and smaller droplets as shown in the EPL for condition OD-45.

SUMMARY AND CONCLUSIONS

X-ray radiography allows quantitative measurements of sprays that are not possible using visible-light or other commonly-available techniques. These measurements provide important information for the design and improvement of rocket injectors. A gas-centered swirl coaxial injector, an injector of relevance to rockets, was used to demonstrate the technique at Argonne National Laboratory's Advanced Photon Source using the 7-BM beamline. This synchrotron source has advantages over laboratory sources, but a mobile flow facility had to be constructed to produce the liquid and gas flow rates needed to simulate liquid rocket injectors.

Two types of measurements were discussed—time-averaged and time-resolved. The time-averaged techniques are relatively rapid, with one, 48.5 mm pass across the width of the spray taking approximately 8 minutes. These measurements provide indications of any asymmetries in the spray along with general information about the spray's evolution in the axial direction. However, care must be taken in interpreting these results for sprays as the discrete nature of the droplets create a dependence on mass flux and velocity. The time-averaged results are able to provide spray widths and mass-averaged velocities, and they show that the GCSC sprays continue to accelerate at least to 20 mm from the injector—the farthest downstream distance interrogated. Since most techniques can only be applied at or beyond this 20 mm distance, the x-ray radiography technique represents a clear improvement and relieves the need to extrapolate data from outside of the combustion zone to the near-injector region of interest.

The time-resolved data provide spray statistics such as droplet size and velocity. However, the line-of-sight nature of the measurement creates complications, especially with the optically-dense sprays investigated. These sprays have several droplets within the beam simultaneously. A simple method was used to extract droplet statistics. Though this method has limitations, qualitative differences in the spray observed using other techniques can be quantified using the x-ray radiography technique. Instabilities in the spray were also measured, and the instability was seen to consist of changes to both the droplet number and size. Improved data acquisition equipment and simple changes to the system will allow improved measurements and minimize the current biases. Overall, while still not perfect, x-ray radiography provides quantitative measurements of dense sprays where all other diagnostics have failed.

ACKNOWLEDGMENTS

A portion of this research was performed at the 7-BM beamline of the Advanced Photon Source, Argonne National Laboratory. Use of the Advanced Photon Source was supported by the U.S. Department of Energy, Office of Science, Office of Basic Energy Sciences, under Contract No. DE-AC02-06CH11357. Daniel Duke (Monash University), Chad Eberhart (University of Alabama, Huntsville), Benjamin Halls (Iowa State University), William Miller (Kettering University) and Christopher Powell (Argonne National Laboratory) assisted in the conduction of the experiments.

REFERENCES

[1] Dexter, C.E., Fisher, M.F., Hulka, J.R., Denisov, K.P., Shibanov, A.A., and Agarkov, A.F., "Scaling Techniques for Design Development and Test," ***Liquid Rocket Thrust Chambers: Aspects of Modeling, Analysis, and Design,*** edited by V. Yang, M. Habiballah, J. Hulka, and M. Popp, Progress in Astronautics and Aeronautics, AIAA, Washington, DC, 2004, pp. 553-600.

[2] Sutton, G.P.; Biblarz, O., **Rocket Propulsion Elements** (7th Edition), John Wiley & Sons, 2001.

[3] Kenny, R.J., Moser, M.D., Hulka, J., Jones, G., "Cold Flow Testing for Liquid Propellant Rocket Injector Scaling and Throttling," *42nd AIAA/ASME/SAE/ASEE Joint Propulsion Conference and Exhibit*, Sacramento, CA, July, 2006.

[4] Ruff, G.A. and Faeth, G.M., "Nonintrusive Measurement of the Structure of Dense Sprays", **Recent Advances in Spray Combustion: Spray Atomization and Drop Burning Phenomena**, edited by Kenneth K. Kuo, Progress in Astronautics and Aeronautics, AIAA, Washington, DC, 1996, pp. 263-296.

[5] Meyer, T.R., Brear, M., Jin, S.H., and Gord, J.R., "Formation and diagnostics of sprays in combustion*,"* **Handbook of Combustion**, Eds. Lackner, M., Winter, F., and Agarwal, A, Wiley-VCH, 2010, pp. 291-322.

[6] Schmidt JB, Schaefer ZD, Meyer TR, Roy S, Danczyk SA, Gord JR., "Ultrafast time-gated ballistic-photon imaging and shadowgraphy in optically dense rocket sprays", *Applied Optics*, Vol. 48, No. 4, pp. B137-44, 2009.

[7] Leick, P., Kastengren, A.L., Liu, Z., Wang, J., and Powell, C.F., "X-ray Measurements of Mass Distributions in the Near-Nozzle Region of Sprays from Standard Multi-Hole Common-Rail Diesel Injection Systems," *11th Triennial International Conference on Liquid Atomization and Spray Systems,* Vail, Colorado, July 2009.

[8] Kastengren, A. L., Powell, C. F., Liu, Z., Moon, S., Gao, J., Zhang, X., and Wang, J., "*Axial Development of Diesel Sprays at Varying Ambient Density*," 22nd Annual Conference on Liquid Atomization and Spray Systems, Cincinnati, Ohio, May 2010.

[9] Lin, K.C., Carter, C., Smith, S., and Kastengren, A., "*Exploration of Aerated-Liquid Jets Using X-Ray Radiography*," 50th AIAA Aerospace Sciences Meeting, Nashville, Tennessee, January 2012.

[10] Halls, B. R., Heindel, T.J., Meyer, T.R., and Kastengren, A.L., "X-ray Spray Diagnostics: Comparing Sources and Techniques," *50th AIAA Aerospace Sciences Meeting, Nashville, Tennessee*, January 2012.

[11] Heindel, T. J., "A Review of X-ray Flow Visualization with Applications to Multiphase Flows," *Journal of Fluids Engineering*, 133-7, (2011).

[12] Schumaker, S. A., Danczyk, S.A., and Lightfoot M.D.A., "Effect of Cup Length on Film Profiles in Gas-Centered Swirl-Coaxial Injectors," *48th AIAA Aerospace Sciences Meeting*, AIAA-2010-368, Orlando, Florida, January 2010.

[13] Schumaker, S. A., Danczyk, S.A., and Lightfoot M.D.A., "Effect of Swirl on Gas-Centered Swirl-Coaxial Injectors," *47th AIAA Joint Propulsion Conference*, AIAA-2011-5621, San Diego, California, July 2011.

[14] Lightfoot, M.D.A., Danczyk, S.A., Watts, J.M., and Schumaker, S.A., "Accuracy and Best Practices for small-scale Rocket Engine Testing," *JANNAF 8th Modeling and Simulation, 6th Liquid Propulsion, and 5th Spacecraft Propulsion Joint Subcommittee Meeting*, Huntsville, Alabama, December 2011, AFRL-RZ-ED-TP-2011-420, ADA554591.

[15] Berger, M.J., Hubbell, J.H., Seltzer, S.M., Chang, J., Coursey J.S., Sukumar, R., Zucker, D.S., and Olsen, K., *XCOM: Photon Cross Sections Database, NIST Standard Reference Database 8 (XGAM)*, http://www.nist.gov/pml/data/xcom/index.cfm.

[16] R2008b, Matlab, MathWorks Inc., 2008.

[17] Strakey, P., Cohn, R. K., and Talley, D., "The Development of a Methodology to Scale between Cold-Flow and Hot-Fire Evaluations of Gas-Centered Swirl Coaxial Injectors," *17th America Annual Conference on Liquid Atomization and Spray Systems*, Arlington, VA, 2004.

[18] Lightfoot, M.D.A., Schumaker, S.A., Villasmil, L.A., and Danczyk, S.A., "The Effect of Swirl on Gas-Centered Swirl Coaxial Injector Sprays," *JANNAF 8th Modeling and Simulation, 6th Liquid Propulsion, and 5th Spacecraft Propulsion Joint Subcommittee Meeting*, Huntsville, Alabama, December 2011, AFRL-RZ-ED-TP-2011-409, ADA554873.

[19] Kastengren, A., Powell, C.F., Wang, Y.-J, IM, K.-S., and Wang, J., "X-ray Radiography Measurements of Diesel Spray Structure at Engine-Like Ambient Density," *Atomization and Sprays*, 19, 1031-1044 (2009).

[20] Lightfoot, M.D.A., Kastengren, A.L., Schumaker, S. A., Danczyk, S. A., and Powell, C.F., "Spray Statistics and Impact of Geometry in Gas-Centered Swirl Coaxial Injectors," *24th Annual Conference on Liquid Atomization and Spray Systems*, San Antonio, TX, May 2012, AFRL-RZ—ED-TP-2012-078, ADA572195.

[21] Lightfoot, M.D.A., Narayanan, V., Kastengren, A.L., Schumaker, S. A., and Danczyk, S.A., "Development of Nonuniformities in Swirling, Rocket Injectors," *24th Annual Conference on Liquid Atomization and Spray Systems*, San Antonio, TX, May 2012, AFRL-RZ-ED-TP-2012-098, ADA571462.

[22] Lefebvre, A.H., **Atomization and Sprays**, CRC Press, 219889.